JACS
JOURNAL OF THE AMERICAN CHEMICAL SOCIETY

Communication

pubs.acs.org/JACS

Label-free Imaging of Neurotransmitter Acetylcholine at Neuromuscular Junctions with Stimulated Raman Scattering

Dan Fu,[†,‡] Wenlong Yang,[‡] and Xiaoliang Sunney Xie*

Department of Chemistry and Chemical Biology, Harvard University, Cambridge, Massachusetts 02138, United States

Supporting Information

ABSTRACT: Acetylcholine is an important neurotransmitter that relays neural excitation from lower motor neurons to muscles. It also plays significant roles in the central nervous system by modulating neurotransmission. However, there is a lack of tools to directly measure the quantity and distribution of acetylcholine at the subcellular level. In this Communication, we demonstrate for the first time that label-free imaging of acetylcholine is achieved with frequency-modulated spectral-focusing stimulated Raman scattering (FMSF-SRS) microscopy: a technical improvement over traditional SRS microscopy that effectively removes imaging backgrounds. Moreover, we directly quantified the local concentration of acetylcholine at the neuromuscular junction of frog *cutaneous pectoris* muscle.

Chemical synapses are fundamental building blocks of neural circuits. They mediate the transfer of signals between different neurons and between neurons and other types of cells such as muscles or glands. The property (excitatory or inhibitory) and efficacy of synaptic signal transmission depends not only on the type of neurotransmitters and receptors but also on the ongoing activity of the synapse itself. The additional complexity of the chemical synapses in comparison to electrical synapses allows for much more complicated behaviors.[1] The imbalance of neurotransmitter levels at the synaptic cleft or defects in neurotransmission are associated with many psychiatric and neurological disorders such as Schizophrenia, depression, Parkinson disease, and Alzheimer disease.[2,3] Therefore, studying neurotransmitter distribution and dynamics in the nervous system are critically important not only for the mapping of neural circuits, but also for revealing the pathophysiology of many neurological diseases and gaining new insights into developing therapeutic treatments.

Despite the pivotal role that neurotransmitters play in neural circuit function, to date, it is still challenging to study them due to the lack of tools that can map their distribution and concentration at the subcellular level. In recent years, there have been intensive efforts in search of engineered fluorescent probes.[4,5] However, because such labels are much bigger than the small neurotransmitter molecules, the results obtained with such labels may not necessarily reflect the behavior of the neurotransmitter themselves. To avoid this problem, label-free approaches were attempted. Maiti et al. performed the first multiphoton fluorescence imaging of serotonin in live cells.[6] However, serotonin fluoresces in the UV range, which could easily be overwhelmed by tissue autofluorescence background.[7] Because of the same reason, fluorescent detection of other neurotransmitters in tissue is even more challenging.

The unique vibrational signatures of neurotransmitter molecules offer the opportunity to image directly neurotransmitters in tissues without the need of labeling. Surface enhanced Raman scattering (SERS) has been used to determine neurotransmitter level in cells.[8] However, the application of SERS in tissue is difficult due to the requirement of colloid nanoparticles for Raman signal amplification. Confocal Raman imaging of neurotransmitters has also been attempted, but is still limited to artificial chemical samples.[9]

In this Communication, we report the first label-free imaging of the neurotransmitter acetylcholine (ACh) in frog muscle with stimulated Raman scattering (SRS) microscopy, an emerging molecular imaging technique.[10−12] ACh is highly concentrated in neuromuscular junctions (NMJ) and acts as the chemical messenger that is released by motor neurons to activate muscles.[13] It also plays critical roles in the central nervous system by functioning as a neuromodulator.[14] We used the intrinsic vibrational signature of ACh at 720 cm^{-1}, corresponding to the symmetric stretching of the C−N bonds of the quaternary ammonium group in choline, to characterize its spatial distribution at the NMJ of frog *cutaneous pectoris* muscle.

Narrowband SRS imaging allows high sensitivity imaging of a particular Raman band defined by the photons' energy difference between the pump and the Stokes lasers. Even though it does not suffer from the nonresonant background that plagues narrow band coherent anti-Stokes Raman scattering (CARS) microscopy, it is not entirely background free. Cross-phase modulation, a nonlinear optical process that is induced by the Kerr effect of the medium, also presents a background that is dependent on the optical alignment and collection efficiency of the pump beam.[15−17] In addition to the purely electronic background, Raman backgrounds are ubiquitously present due to many Raman active modes of lipids, proteins, and nucleic acids in the fingerprint region.[18] Even though ACh concentration is relatively high at the NMJ, the backgrounds still dominate the measurement. To image a neurotransmitter, ACh in particular, we developed a frequency-modulation spectral-focusing SRS (FMSF-SRS) technique. It combines the advantages of the spectral focusing method,[19]

Received: October 13, 2016
Published: December 27, 2016

DOI: 10.1021/jacs.6b10727
J. Am. Chem. Soc. 2017, 139, 583−586

which improves sensitivity, and the frequency modulation method,[16,20] which provides real-time background subtraction.

Figure 1 shows the schematic of the FMSF-SRS setup. It is similar to the hyperspectral SRS imaging setup[19] and

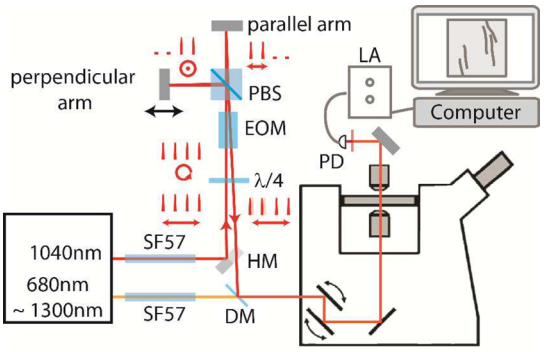

Figure 1. Schematic diagram of FMSF-SRS. SF57, SF57 glass rods; PBS, polarizing beam splitter; EOM, electro-optic modulator; $\lambda/4$, quarter-wave plate. HM, D-shape half mirror; DM, dichroic mirror; PD, amplified photo diode.[21] LA, lock-in amplifier. Arrows below the pulses indicate their polarization.

frequency-modulation CARS setup.[20] In short, the two outputs of an Insight DeepSee laser were sent through long SF57 glass rods (total length of 54−60 cm) to stretch the laser pulses to 2−3 ps. The 1040 nm laser (Stokes beam) was synchronously polarization modulated by a resonant electro-optic modulator (EOM) driven at 20 MHz. Every two laser pulses passed through a polarizing beam splitter (PBS) and reflect back by a mirror (parallel arm), whereas the next two pulses were reflected by PBS and then sent back by a different mirror on a translation stage (perpendicular arm). Beams on both arms were amplitude modulated, but when combined together after transmitting back through PBS and EOM, they appeared nonmodulated in amplitude. Frequency modulation was achieved by adjusting the time delay of the two arms of the Stokes beam, because in spectral-focusing SRS, Raman frequency is linearly dependent on the time delay of the pump and the Stokes beam. When the perpendicular arm is blocked, we revert back to the hyperspectral spectral-focusing SRS imaging setup.

We first determined the detection linearity and sensitivity of ACh at the 720 cm^{-1} Raman peak using the hyperspectral SRS setup (Figure 2A,B). The detection limit is about 20 mM at a lock-in integration time of 4 μs. This is close to the 30 mM concentration of ACh in frog NMJ estimated previously.[13] 20 mM is the sensitivity for a single pixel in a single image. If averaging is used and pixels are combined together, as in the case of imaging of ACh in NMJs of frog, the sensitivity can be much higher. At such concentration, the background signal could easily overwhelm the Raman signal from ACh. In pure solutions, only after subtraction of the background, SRS signals are linearly proportional to concentrations of ACh (Figure 2C). However, in live tissue, the background signal is nonuniform and changes over time due to sample movement, necessitating real-time background subtraction using FMSF-SRS.

Next, we demonstrated how frequency modulation technique can effectively remove the backgrounds, which have a much broader spectral distribution than the 720 cm^{-1} Raman peak of the ACh. At a certain relative delay between pump and Stokes laser, the Stokes pulses that went through the parallel arm and

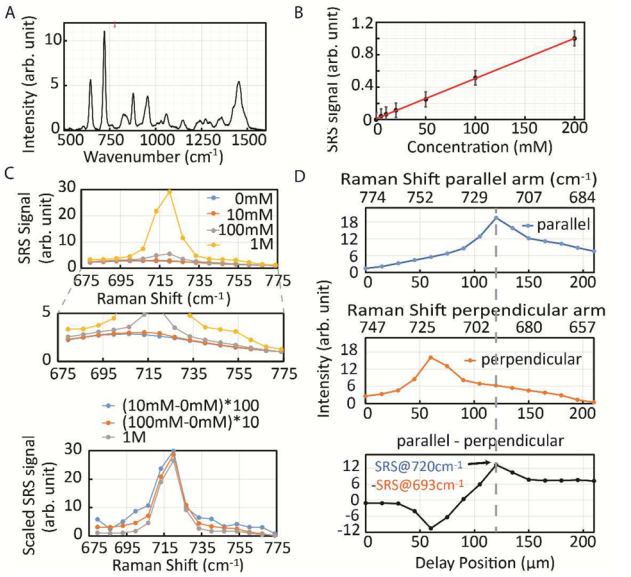

Figure 2. Spectral characterization of ACh by spontaneous Raman and SRS. (A) Spontaneous Raman spectrum of ACh. (B) Concentration curve of ACh measured by hyperspectral spectral-focusing SRS. The error bar shows the noise level on the images. (C) Spectral focusing SRS spectral scan of ACh at different concentrations. The middle figure shows the zoomed in intensity profile at lower concentrations and the bottom figure shows the SRS spectra of ACh after subtracting water background. (D) Hyperspectral SRS scan of individual arms and the FMSF-SRS spectral scan signal when both arms are used.

the perpendicular arm of our FMSF-SRS setup gave rise to signals of different Raman frequency. Because their modulation phase differ by 180°, their SRS signal was directly subtracted in the lock-in amplifier and resulted in a frequency modulated SRS signal. By scanning the relative delay between pump and Stokes beams, we obtained an FMSF-SRS spectrum of 100 mM ACh in solution (Figure 2D). We note that FMSF-SRS is analogous to derivative Raman spectroscopy of the first order and shift excitation Raman spectroscopy, which have been employed to remove fluorescence background.[22,23] The signal of FMSF-SRS is identical to that obtained through direct subtraction of two SRS signals at different wavenumbers. However, FMSF-SRS performs the derivative operation optically in real time instead of digitally during postprocessing, offering a significant advantage of resistance to sample movement and pump power fluctuation. These advantages lead to better signal fidelity and higher signal-to-noise ratio.

We applied our imaging technique to study the frog NMJ. We used adult *Rana pipiens*, a common North American leopard frog, as our experimental model. The animal was anesthetized and sacrificed following the animal protocol approved by Harvard University Institutional Animal Care and Use Committee. The *cutaneous pectoris* muscles were dissected for imaging and electrophysiology experiments following the protocol described by Wu et al.[24] The location of *cutaneous pectoris* muscle and structure of frog NMJ is shown in Figure 3A. The neurotransmitter ACh is stored in synaptic vesicles with an average size of ∼40 nm. Because the spatial resolution of microscope is limited to ∼300 nm, we imaged the whole synaptic vesicle pool[25,26] in the focal volume instead of individual vesicles. To locate the NMJ in the frog *cutaneous pectoris* muscle, we used alpha-Bungarotoxin-Alexa488 (α-BTX-Alexa488) staining. α-BTX binds to the ACh receptors of NMJ

DOI: 10.1021/jacs.6b10727
J. Am. Chem. Soc. 2017, 139, 583−586

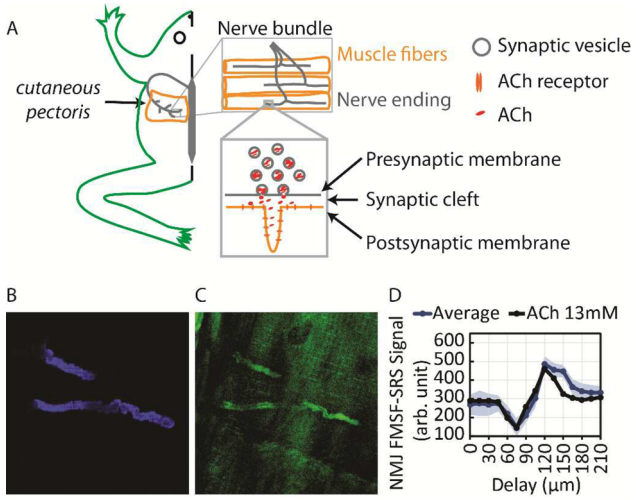

Figure 3. Frog NMJ structure and imaging with FMSF-SRS. (A) Cartoon diagram of frog muscle dissection and the anatomical structure of NMJs. (B) α-BTX staining of the NMJ. (C) FMSF-SRS image of the NMJ. (D) Hyperspectral FMSF-SRS data of the NMJs compared with that of a 13 mM ACh solution.

that are closely located with vesicles containing ACh. A two-photon fluorescence images of α-BTX-Alexa488 excited with the same lasers for SRS is shown in Figure 3B. Indeed, they colocalized with the FMSF-SRS images of ACh shown in Figure 3C. The frequency modulation reduced the background by about 3- to 4-fold as shown in Figure S1. The background in FMSF-SRS was also flatter than the spectral-focusing SRS image taken without frequency modulation. Detailed imaging parameters are provided in the Supporting Information.

It is important to note that acetylcholine is not the only species that has the 720 cm^{-1} Raman peak we are probing. It is known that phosphatidylcholine that contains choline is present in the membrane of synaptic vesicles. It is estimated that there are 2524 phosphatidylcholine molecules in each synaptic vesicle.[27] Even though this number is much smaller compared with 11 000 ACh in each vesicle,[28] it is still contributing to the measured FMSF-SRS signal. Because vesicular membrane and vesicular acetylcholine are colocalized and cannot be resolved due to insufficient spatial resolution, the obtained FMSF-SRS image contains both species.

To verify that the detected SRS signal largely came from ACh and to estimate its concentration, we performed hyperspectral FMSF-SRS imaging of the muscle tissue. After subtracting the signal of nearby muscle, we obtained the spectra of the NMJs in Figure 3D. The solid blue line shows the average SRS signal level at each delay and it matches the signal of a 13 mM ACh solution (black line). The result is based on the measurement of 14 NMJs from 5 animals. If we consider the contribution from both ACh and phosphatidylcholine, the concentration of ACh will be ~10 mM, which is close to previously published data.[13]

Interestingly, the difference between the two-photon fluorescence image of the ACh-receptors and the FMSF-SRS image of ACh vesicles highlights the architecture of NMJ. In frog NMJ, ACh receptors on the muscle cell spread around the docking sites of synaptic vesicles. Therefore, the fluorescence images of the ACh-receptors appear wider than images of ACh in the vesicles in Figure 3B,C. We further performed a 3-D Z-stack imaging to verify the structure. As shown in Figure S2, the receptors enclosed the vesicles in the axon terminals.

Lastly, we performed control experiments to corroborate that when vesicles release ACh, SRS signal will decrease. It is known that strong electrical excitation will force the vesicles at NMJs to release neurotransmitters.[24] After exciting the neuromuscular junction with a 20 Hz square wave at 4 V for 10 min, the majority of the ACh in the vesicles should be released and diffused out, but an empty vesicular structure remained, which was stained with FM1-43 dye that were taken in during membrane fusion between the vesicles and the cell membrane. The imaging results are shown in Figure 4. We observed that

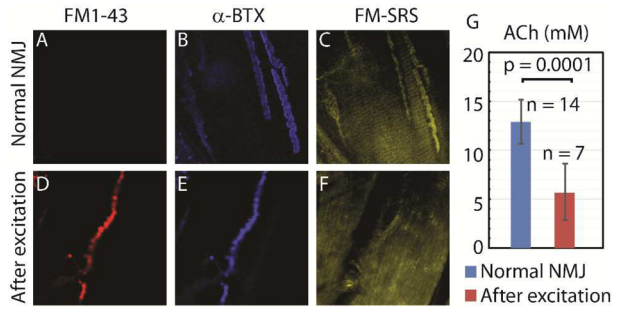

Figure 4. Images and characterization of frog NMJs with and without strong electrical stimulation. (A, D) Two-photon fluorescence image of FM dye excited by 1040 nm laser without and with electrical excitation. (B, E) Two-photon fluorescence image of α-BTX staining excited by 970 nm laser without and with electrical excitation. (C, F) FMSF-SRS image of NMJs without and with electrical excitation. (G) Comparison of choline concentrations between unstimulated NMJs and NMJs after strong electrical stimulation. The error bars show the standard deviations. The p-value is calculated from one-tail unpaired student t test.

after excitation, α-BTX staining remains, and FM dye staining became visible. The FMSF-SRS signal of ACh had greatly decreased in NMJs with strong electrical excitation compared to normal NMJs without electrical excitation.

We recorded the FMSF-SRS spectra of the NMJs after excitation, and compare them with that of unexcited NMJs (Figure 4G). We found that the average concentration of choline group in the NMJ has decreased from 12.9 to 5.7 mM. This provided a lower limit of 7.2 mM of ACh concentration in NMJ. The control experiments further demonstrated that the FMSF-SRS signal of NMJs originated mostly from ACh in vesicles, and ACh concentration was significantly reduced when it was released from vesicles. The residue signal may have several sources, the most significant one being the phosphatidylcholine in vesicular membranes.

To summarize, we demonstrated for the first time that using vibrational contrast the neurotransmitter acetylcholine can be directly visualized and accurately measured in tissue. This proof-of-principle experiment illustrated the power of label-free SRS imaging. This same approach could potentially be used for imaging other important neurotransmitters such as dopamine, serotonin, glutamate, GABA etc. Compared with multiphoton fluorescence imaging,[6] SRS uses longer wavelength and longer pulses, and therefore is less damaging to live cells and tissues. However, for imaging of neurotransmitters in the central nervous system, where synapses are much smaller than those in NMJ,[29] further improvement in sensitivity will be necessary. One major hurdle is that the background signal in tissues is not

DOI: 10.1021/jacs.6b10727
J. Am. Chem. Soc. 2017, 139, 583−586

completely removed by frequency modulation. For a relatively flat Raman background, frequency modulation can reduce the background well. However, when the Raman background has peaks around the Raman frequency we use for imaging, it cannot be effectively suppressed. Other published frequency modulation schemes suffer from the same problem.[16] It is possible to use a broader spectrum instead of two Raman bands to suppress Raman background signal further, e.g., using spectral-tailored excitation SRS[30] or spectral encoded SRS.[31]

We note that the ACh measured by FMSF-SRS in muscles includes the reserve pool, recycling pool and ready release pool. Because the reserve pool consists of 80% of synaptic vesicles, our experiments were mainly visualizing the reserve pool.[25] Further study of vesicle release from the ready release pool of the NMJ are currently limited by the sensitivity of FMSF-SRS. We postulate that with further improvement of sensitivity of SRS, this method may open up new avenues for *in vivo* study of synaptic activity.

■ ASSOCIATED CONTENT

Supporting Information

The Supporting Information is available free of charge on the ACS Publications website at DOI: 10.1021/jacs.6b10727.

Imaging experiment details, XYZ scan of NMJ with FMSF-SRS and laser filter choice for two-photon fluorescence imaging (PDF)

■ AUTHOR INFORMATION

Corresponding Author

*xie@chemistry.harvard.edu

ORCID

Xiaoliang Sunney Xie: 0000-0001-7714-9776

Present Address

†Department of Chemistry, University of Washington, Seattle, Washington, 98195, United States.

Author Contributions

‡These authors contributed equally

Notes

The authors declare the following competing financial interest(s): X.S.X. is a cofounder of Invenio Imaging, a start-up for SRS microscopy. Other authors declare no competing financial interests.

■ ACKNOWLEDGMENTS

We thank Dr. William Betz and Dr. Achim Klug for kindly training us to perform the frog pectoral muscle dissection and providing us the electrical excitation device. We thank Dr. Patricia Purcell's help on revising the paper. This research is supported by DOE Lipid (DE-SC0012411) and DOE SISGR (DE-SC0001548).

■ REFERENCES

(1) Branco, T.; Staras, K. *Nat. Rev. Neurosci.* **2009**, *10*, 373.
(2) Coyle, J.; Price, D.; DeLong, M. *Science* **1983**, *219*, 1184.
(3) Lipton, S. A.; Kater, S. B. *Trends Neurosci.* **1989**, *12*, 265.
(4) Gubernator, N. G.; Zhang, H.; Staal, R. G. W.; Mosharov, E. V.; Pereira, D. B.; Yue, M.; Balsanek, V.; Vadola, P. A.; Mukherjee, B.; Edwards, R. H.; Sulzer, D.; Sames, D. *Science* **2009**, *324*, 1441.
(5) Marvin, J. S.; Borghuis, B. G.; Tian, L.; Cichon, J.; Harnett, M. T.; Akerboom, J.; Gordus, A.; Renninger, S. L.; Chen, T.-W.; Bargmann, C. I.; Orger, M. B.; Schreiter, E. R.; Demb, J. B.; Gan, W.-B.; Hires, S. A.; Looger, L. L. *Nat. Methods* **2013**, *10*, 162.
(6) Maiti, S.; Shear, J. B.; Williams, R. M.; Zipfel, W. R.; Webb, W. W. *Science* **1997**, *275*, 530.
(7) Tan, W.; Parpura, V.; Haydon, P. G.; Yeung, E. S. *Anal. Chem.* **1995**, *67*, 2575.
(8) Dijkstra, R. J.; Scheenen, W. J. J. M.; Dam, N.; Roubos, E. W.; ter Meulen, J. J. *J. Neurosci. Methods* **2007**, *159*, 43.
(9) Manciu, F. S.; Lee, K. H.; Durrer, W. G.; Bennet, K. E. *Neuromodulation* **2013**, *16*, 192.
(10) Freudiger, C. W.; Min, W.; Saar, B. G.; Lu, S.; Holtom, G. R.; He, C. W.; Tsai, J. C.; Kang, J. X.; Xie, X. S. *Science* **2008**, *322*, 1857.
(11) Fu, D.; Zhou, J.; Zhu, W. S.; Manley, P. W.; Wang, Y. K.; Hood, T.; Wylie, A.; Xie, X. S. *Nat. Chem.* **2014**, *6*, 614.
(12) Cheng, J.-X.; Xie, X. S. *Science* **2015**, *350*, aaa8870.
(13) Israel, M.; Dunant, Y.; Manaranche, R. *Prog. Neurobiol.* **1979**, *13*, 237.
(14) Picciotto, M. R.; Higley, M. J.; Mineur, Y. S. *Neuron* **2012**, *76*, 116.
(15) Fu, D.; Ye, T.; Matthews, T. E.; Yurtsever, G.; Warren, W. S. *J. Biomed. Opt.* **2007**, *12*, 054004.
(16) Zhang, D.; Slipchenko, M. N.; Leaird, D. E.; Weiner, A. M.; Cheng, J.-X. *Opt. Express* **2013**, *21*, 13864.
(17) Andreana, M.; Houle, M.-A.; Moffatt, D. J.; Ridsdale, A.; Buettner, E.; Légaré, F.; Stolow, A. *Opt. Express* **2015**, *23*, 28119.
(18) Puppels, G. J.; de Mul, F. F. M.; Otto, C.; Greve, J.; Robert-Nicoud, M.; Arndt-Jovin, D. J.; Jovin, T. M. *Nature* **1990**, *347*, 301.
(19) Fu, D.; Holtom, G.; Freudiger, C.; Zhang, X.; Xie, X. S. *J. Phys. Chem. B* **2013**, *117*, 4634.
(20) Chen, B.-C.; Sung, J.; Lim, S.-H. *J. Phys. Chem. B* **2010**, *114*, 16871.
(21) Tian, F.; Yang, W.; Mordes, D. A.; Wang, J.-Y.; Salameh, J. S.; Mok, J.; Chew, J.; Sharma, A.; Leno-Duran, E.; Suzuki-Uematsu, S.; et al. *Nat. Commun.* **2016**, *7*, 13283.
(22) Van de Ven, M.; Meijer, J.; Verwer, W.; Levine, Y.; Sheridan, J. *J. Raman Spectrosc.* **1984**, *15*, 86.
(23) Martins, M. A. d. S.; Ribeiro, D. G.; Pereira dos Santos, E. A.; Martin, A. A.; Fontes, A.; Martinho, H. d. S. *Biomed. Opt. Express* **2010**, *1*, 617.
(24) Wu, L. G.; Betz, W. J. *Neuron* **1996**, *17*, 769.
(25) Rizzoli, S. O.; Betz, W. J. *Nat. Rev. Neurosci.* **2005**, *6*, 57.
(26) Rizzoli, S. O.; Betz, W. J. *Science* **2004**, *303*, 2037.
(27) Takamori, S.; Holt, M.; Stenius, K.; Lemke, E. A.; Grønborg, M.; Riedel, D.; Urlaub, H.; Schenck, S.; Brügger, B.; Ringler, P. *Cell* **2006**, *127*, 831.
(28) Miledi, R.; Molenaar, P. C.; Polak, R. L. *J. Physiol.* **1982**, *333*, 189.
(29) Houser, C. R. *J. Electron Microsc. Tech.* **1990**, *15*, 2.
(30) Freudiger, C. W.; Min, W.; Holtom, G. R.; Xu, B.; Dantus, M.; Sunney Xie, X. *Nat. Photonics* **2011**, *5*, 103.
(31) Liao, C.-S.; Wang, P.; Wang, P.; Li, J.; Lee, H. J.; Eakins, G.; Cheng, J.-X. *Sci. Adv.* **2015**, *1*, e1500738.

DOI: 10.1021/jacs.6b10727
J. Am. Chem. Soc. 2017, 139, 583−586